ANATOMICAL CORRELATES TO THE BANDS SEEN IN THE OUTER RETINA BY OPTICAL COHERENCE TOMOGRAPHY:

Literature Review and Model

RICHARD F. SPAIDE, MD[*,†] and **CHRISTINE A. CURCIO, PhD**[‡]

[*]Vitreous-Retina-Macula Consultants of New York, New York

[†]LuEsther T. Mertz Retinal Research Center, Manhattan Eye, Ear & Throat Hospital, New York, New York

[‡]Department of Ophthalmology, Callahan Eye Foundation Hospital, University of Alabama School of Medicine, Birmingham, Alabama

Abstract

Purpose—To evaluate the validity of commonly used anatomical designations for the four hyperreflective outer retinal bands seen in current-generation optical coherence tomography, a scale model of outer retinal morphology was created using published information for direct comparison with optical coherence tomography scans.

Methods—Articles and books concerning histology of the outer retina from 1900 until 2009 were evaluated, and data were used to create a scale model drawing. Boundaries between outer retinal tissue compartments described by the model were compared with intensity variations of representative spectral-domain optical coherence tomography scans using longitudinal reflectance profiles to determine the region of origin of the hyperreflective outer retinal bands.

Results—This analysis showed a high likelihood that the spectral-domain optical coherence tomography bands attributed to the external limiting membrane (the first, innermost band) and to the retinal pigment epithelium (the fourth, outermost band) are correctly attributed. Comparative analysis showed that the second band, often attributed to the boundary between inner and outer segments of the photoreceptors, actually aligns with the ellipsoid portion of the inner segments. The third band corresponded to an ensheathment of the cone outer segments by apical processes of the retinal pigment epithelium in a structure known as the contact cylinder.

Conclusion—Anatomical attributions and subsequent pathophysiologic assessments pertaining to the second and third outer retinal hyperreflective bands may not be correct. This analysis has identified testable hypotheses for the actual correlates of the second and third bands. Nonretinal pigment epithelium contributions to the fourth band (e.g., Bruch membrane) remain to be determined.

Keywords

anatomy; histology; optical coherence tomography; retina; macula

Optical coherence tomography (OCT) made possible noninvasive visualization of the microscopic anatomy of the retina, a nearly transparent structure. Understanding what is visualized requires proper identification of the layers and substructures within the retina.

Reprint requests: Richard F. Spaide, MD, 460 Park Avenue, 5th Floor, New York, NY 10022; rickspaide@gmail.com.

Comparatively low resolution early OCT devices detected one highly reflective band (or "line") in the posterior ocular fundus. This band was ascribed to more than one structure depending on the authority.[1–6] Introduction of commercial OCT devices occurred in 1996, and initially the retinal thickness was measured from the inner retina to the top of the highly reflective posterior band.[4,5] Development of higher-bandwidth illumination in research devices increased attainable resolution to 3 μm to 4 μm and was called "ultrahigh-resolution" OCT. With the newer OCTs, the formerly single highly reflective band was resolved as either three or four separate bands. Various publications attributed diverse anatomical correlates to these bands; the discordance existed not only between different author groups but also between papers from the same group.[7–9] The 2007 entry into the commercial market and subsequent widespread adoption of high-resolution spectral-domain OCT created the opportunity for practicing ophthalmologists to have a nearly cellular level of resolution of the retina.[10] A practical need for terminology of various layers of the retina arose and an ad hoc nomenclature, based on an amalgamation of previous OCT papers, was adopted by the ophthalmic community.

Commercial spectral-domain OCT instruments conventionally resolve 4 bands in the outer retina outside of the central fovea (Figure 1). The innermost band has been attributed to the external limiting membrane (ELM),[8] a linear confluence of junctional complexes between Muller cells and photoreceptors. This band typically is thinner and much fainter than the others. The second of the four bands has been commonly ascribed to the boundary between the inner segments (IS) and outer segments (OS) of the photoreceptors.[9,11] The third band is commonly referred to as either the OS tips[12] or as Verhoeff membrane.[13,14] The outermost highly reflective band has been thought to represent the retinal pigment epithelium (RPE), Bruch membrane, and possibly the choriocapillaris.[2,6,8,14,15]

Close inspection of these four bands raises questions about some of these assignments. For both foveal cones and rods, the length of the OSs is roughly the same as the ISs,[16,17] so one would expect the boundary between the IS and OS to lie at the midpoint between the ELM and RPE. However, the second reflective band lies much closer to the ELM than it does to the RPE. Further, the word "boundary" implies a narrow line as a reflection, while the "IS/OS boundary" image typically is nearly as thick as the RPE band. Finally, although the third band is called Verhoeff membrane, what Verhoeff described was an anatomical structure girdling RPE cells,[18,19] known now as junctional complexes between RPE cells.[20,21] Therefore, a reflective band physically separated from the RPE cannot be Verhoeff membrane.

Over the last century a wealth of information about the anatomical structure of the retina has been published, complete with meticulous measurements. Assembling this information into a database would allow comparisons between known measurements and the structures seen by OCT. We assembled this information and constructed a scale model drawing of the outer retina to enable visual comparisons. Using this model for analysis, we find that the designation of the ELM for the first band is correct and that the fourth band at least contains the RPE, but current assignments of the middle two bands are more problematic.

Methods

Original literature from 1900 until 2009 describing the histology of the retina were reviewed to find relevant information for a database of representative values (Table 1). Repetitive or derivative works were not used. This assembled information, along with the photomicrographs in the publications, was used to create drawings of the outer retina using CorelDRAW X5 (Corel Corporation, Ottawa, Canada). The drawings were made to scale, with equal horizontal and vertical scaling. Three representations were made of

photoreceptors: cones from the central fovea and rods and a cone from the perifoveal region (as per Polyak,[35] 2 mm temporal to the fovea). In the drawing, junctional complexes between the Muller cells and the photoreceptors, which in aggregate form the ELM, were labeled as the ELM. Similarly the junctional complexes girdling the RPE cells were labeled "Verhoeff membrane" to be consistent with past histologic nomenclature.

Drawings were compared with a representative scan obtained of one of us (R.F.S.) using the Heidelberg Spectralis HRA+OCT (Heidelberg Engineering, Vista, CA) in high-resolution mode. This instrument has an axial resolution of approximately 7 μm. A longitudinal reflectance profile (LRP) from a horizontal scan taken through the fovea center was created by averaging pixels across at each level of 10 adjacent A-scans using ImageJ (Version 1.44f; National Institutes of Health, Bethesda, MA). Additional scans were obtained of other subjects that did not differ from what is shown in this report and scans obtained with the Cirrus HD-OCT (Carl Zeiss Meditec, Dublin, CA), which also showed similar results. Therefore, only one scan will be shown in the comparison to the model. The LRPs were determined from the display information of the Heidelberg Spectralis.

Considerations Concerning the Appearance of Bands as Imaged by Optical Coherence Tomography—Image Transformations

Optical coherence tomography instruments do not display raw information because of the huge dynamic range of the underlying amount of backscattering detected in making the image, which has the potential to exceed 100,000:1. As illustrated by Weber law,[54] the number of gradient steps human sensory systems can detect is limited, often to 20 or 30 discrete steps. By convention a mathematical transformation of the underlying linear OCT data is made, be it logarithmic, root, or combination of the two to compress the information into a form the human visual system can use.[1,55] Because of this compression, any of these transforms would tend to increase the widths of the hyperreflective bands (Figure 2). In addition to alterations because of this transform, widths of bands are also influenced by the axial point spread function (PSF) of the OCT instrument, which in turn is generally equivalent to the axial resolution.[56]

Point Spread Function

An infinitely thin reflector would be imaged as having a thickness equivalent to the PSF of the OCT instrument, because the output image is the convolution of the PSF with the reflector.[56] Thus, an infinitely thin reflector would appear 7 μm thick with the Spectralis. The greater the thickness of the imaged object, the smaller the measurement error attributable to the PSF of the instrument. In a simplified situation, an object with a Gaussian reflectance profile of thickness T_O imaged by an OCT with a Gaussian PSF will produce an image with a thickness $T_I = (T_O^2 + PSF^2)^{1/2}$. In confocal microscopy, the PSF is measured using test objects, because the actual value frequently is different and less favorable than the theoretical one and the measured value is used in deconvolution calculations.[57] In OCT measurement of the actual PSF is not commonly done, probably because the PSF is highly influenced by aberrations in the eye being imaged, which vary from one person to the next and because there is no suitable way to introduce a test object into a person's eye in the first place.

Results

Description of Outer Retinal Cells

Central foveal cones and retinal pigment epithelium—Anatomical measurements assembled from the literature are shown in Table 1. The outer retinal drawing illustrating the central foveal cones and their relationship to the RPE is shown in Figure 3A. As shown in

Figure 3B, a higher-magnification panel, foveal cones are narrow, nearly cylindrical, and have some rodlike morphology. Photoreceptor IS are divided into two parts, the myoid (near the ELM) and the ellipsoid (near the OS). The myoid has ribosomes, some endoplasmic reticulum, Golgi bodies, and rare mitochondria. The ellipsoid is densely packed with mitochondria. Unlike the kidney-shaped mitochondria found scattered in a typical cell, those in the IS ellipsoid are long, thin ($\sim$0.25 × 3 μm) and tightly packed in parallel, like a bundle of uncooked spaghetti. The unusual size, orientation, and arrangement of these mitochondria suggest that they could confer an optical benefit beyond their role in energy production. The link between the IS and OS is a narrow passage containing the connecting cilium, a structure 0.25 μm by 1 μm having a 9+0 configuration of microtubules, much the same as other nonmotile cilia in the rest of the body.

Muller cells terminate at the inner border of the IS myoids. Junctional complexes between the Muller cells and the photoreceptors when seen in aggregate form the ELM. Muller cells have apical projections that extend beyond the ELM. At the outer end of the ellipsoids are fine specialized microvilli with a rigid actin core called calycal (or calyceal) processes that overlap the proximal OS. The OS extend to the RPE with a slight taper. They stop just short of the RPE cell surface to create a gap called the supracone space.

The RPE cell has microvilli, which are apically extending, fingerlike extensions that frequently contain melanosomes. More prominent processes wrap around the cone OS tips to create a contact cylinder. Retinal pigment epithelium cells in the central macula are taller and have more melanosomes than RPE cells located peripherally. Retinal pigment epithelium organelles are spatially segregated within the cytoplasm, with melanosomes predominant in the apical compartment and nuclei and mitochondria predominant in the basal compartment. Encircling each RPE cell near its apical surface is a ring of junctional complexes, first identified by Verhoeff, that form the outer blood–retina barrier. Analogous to naming the confluence of junctional complexes between Muller cells and photoreceptors a membrane, the RPE junctional complexes were called Verhoeff membrane.

Perifoveal cones and retinal pigment epithelium—With increasing eccentricity, cone IS become shorter and wider (Figure 4). Mitochondria are more completely segregated into the ellipsoid and their packing density increases.[36] Approximately 75% of ellipsoid volume is accounted for by mitochondria, unique among cells in the body. Because of increased IS width, IS are more sharply tapered toward the OS. The calycal processes extend 1 μm along the OS. The taper of the OS toward the RPE is somewhat more prominent than that seen in foveal cones. Outer segment of nonfoveal cones terminate well above the RPE to form a large supracone space. Within this space, long RPE apical processes envelope the outer 1/3 of cone OS to form a contact cylinder.[16] Relative to RPE microvilli, these ensheathing processes have more cellular machinery, including mitochondria and ribosomes, in addition to melanosomes. Shed OS are propelled by peristaltic-like activity of these long processes toward the RPE cell body.[39] With age, a widening and shortening of cones enlarges the supracone space, particularly near the optic nerve.[23,58] Retinal pigment epithelium cells demonstrate the microvilli, junctional complexes, and intracellular contents seen in the fovea.

Rods—Rods are narrower and more cylindrical than cones outside of the central fovea (Figure 5). The mitochondrial packing density is somewhat lower for rods than neighboring cones. The calycal processes are generally longer, show more variation in length, and are less numerous for rods than for cones. The OS of rods abut the RPE cell bodies, and electron microscopy is needed to accurately measure any gap between the two cell types. The apical processes surrounding the rod OS tips are more diaphanous than those surrounding cone OSs.

Determining the Origin of the Reflective Bands

External limiting membrane—The thinness of the histologic ELM requires incorporating knowledge about how its apparent width is changed in OCT. The required location and thinness of the reflector are both consistent with the Muller cell junctional complexes of the ELM being the origin of the signal for Band 1, although it is possible that Muller cell microvilli could contribute to the width of the band.

Retinal pigment epithelium—The fourth hyperreflective outer retinal band has been attributed to the RPE, with potential contribution from Bruch membrane and the choriocapillaris. Abundant experimental and clinical evidence supports this designation, including histologic–OCT correlation in animal eyes[15,59] and excimer laser ablation of human and bovine retinas.[60] Defects corresponding to the RPE monolayer with increased signal backscattering from the underlying choroid have been seen in eyes with RPE tears.[61,62] Increased signal penetration past the fourth band is seen in cases of RPE atrophy.[63] Congenital hypertrophy of the RPE produces an exaggerated signal corresponding to the fourth band.[64] Because of scattering by melanosomes, a scrambling of polarization of the probing beam is expected and is considered a characteristic finding.[65,66] This specific tissue–light interaction has led to the suggestion that polarization-sensitive OCT could be used to identify and segment the RPE.[67] This method of imaging identifies the RPE as being the major component of the fourth band.

The second and third bands—The nomenclature for the middle two bands have significantly less supportive evidence, particularly in view of shifting interpretations of these bands over time. Because our outer retina model was made to scale, it is straightforward to compare it with representative OCT scans using the LRP analysis (Figure 6 for fovea, Figure 7 for perifovea). In these comparisons, Band 1 of the OCT was aligned to the ELM in the model, and Band 4 in the OCT image was aligned with the RPE. Specifically, the fourth band peak from the LRP was aligned with the apical RPE, the predominant location of melanosomes.

The results of this analysis were consistent for both the fovea and perifovea. In both regions the second reflective band colocalized with the ellipsoid section of the model. In contrast, the LRP for this band reached a nadir near the IS/OS boundary. The third reflective band aligned with the region of the distal portion of the cone OS, where the model indicates the presence of the contact cylinder. The third band typically merges with the fourth band in the central fovea, where the cone OS tips and consequently the contact cylinder are closely apposed to the RPE cell body.

Discussion

Detailed anatomical data were assembled from past publications into a small database of values. This information was used to make a scale drawing. Using analysis of the available data, it appears likely that reassignment of the anatomical correlates of the bands in the outer retina will be needed. From this preliminary analysis, the 4 outer bands seen in a typical spectral-domain OCT scan in order are the ELM, the ellipsoid section of the photoreceptors, the contact cylinder of the cones, and finally the RPE. While a drawing is not likely to be the final arbiter of band assignments, the findings of the present study suggest that current assignments of Bands 2 and 3 are not correct and additional work needs to be done. This includes methodology to extract actual band thicknesses from the raw OCT data before any transformation is used to display the data and detailed light and electron microscopic analysis of layer thicknesses in the retina. We have begun these projects based on the findings of this preliminary study. Correct band assignment will aide in proper evaluation of

both normal and pathologic states in the retina. Early adoption of naming systems for the outer bands provided a way to communicate anatomical findings, but incorrect assignment may pose problems. After adoption of naming assumptions, it is common to base conclusions on these corresponding anatomical correlates in assessing retinal anatomy and pathophysiology. These secondary conclusions and assumptions would need to be revised as well.

In addition to anatomical correlations visible by comparing the OCT images with the drawing, there are other factors that can be used to help validate some of the conclusions. The second band seen in OCT images has commonly been attributed to the IS/OS boundary. A boundary imaged by OCT should have a thickness as influenced by the PSF and the variation in how the various cellular features align with each other. However, the anatomy of the transition between the ISs and OSs raises concerns. First for cones there actually is no sharp boundary. Cone OS disks are actually comblike projections of the plasma membrane that start in steps near the IS. Rod OS are plasma membrane-bounded stacks of disks clearly separate from the IS and connected to it by the cilium. Second, extensions of the ellipsoid cytoplasm over the OSs (the calycal processes) would have the optical characteristic of blurring the boundary of refractive index change. This strategy is used to reduce reflection in optical design.[67] Third, an increasing deviation from normal occurs for light rays striking photoreceptors with increasing eccentricity; the nodal point of the eye is anteriorly displaced to the radius of the retinal surface.[34] This would decrease the reflection with increasing displacement from the optical axis. The reflective potential of the "boundary" would be enhanced if it actually were a sharp transition. Even making this assumption, the proportion of incident light reflected (L_R) for light normal to the boundary can be approximated by the Fresnel equation as $L_R = ((n_I - n_O)/(n_I + n_O))^2$, where n_I is the refractive index of the ISs and n_O is the refractive index of the OS. Given the known refractive indexes (as shown in the Table 1), the proportion of light reflected by a boundary would be approximately 0.00021% for cones and 0.00012% for rods. This result is not entirely unexpected because it would not be efficient for a light receptor system to reflect light. Thus, ascribing one of the brightest OCT bands in the posterior fundus to a region with an extremely low reflectance is not likely to be correct. In addition, a boundary should have an observed thickness close to the PSF of the OCT instrument. The second band is usually nearly as thick as the fourth band, which represents at least the thickness of an entire RPE cell (10–14 μm). Finally, because of its very small size, one other candidate for the second band, the connecting cilium,[68] would not be visible using OCT. The cilium is outnumbered by a factor greater than 100:1 by the IS mitochondria, which also makes it difficult to ascribe any significant observable reflection arising from the cilium.

Band 3 in the OCT appears to correspond to the contact cylinder between the RPE apical processes and the external portion of the cone OS. This layer is clearly not Verhoeff membrane. It also, strictly speaking is not the photoreceptor tips, which would imply the reflection only comes from the ends of the OS. The third band has a definite thickness and so the reflection must come from a region, not a boundary. Some investigators have claimed that outside of the central macular region, the cone OS tips and rod OS tips (what they called ROST) formed different bands in OCT images.[69,70] Curiously the layer termed COST in these reports was not a discrete band in higher-magnification illustrations.[69,70] However, the rod OS terminate at the RPE at a distance well below the resolution of OCT, and thus could not be detected as a band distinct from the fourth band by OCT. In addition, if the rod OS tips were visible, one would expect some degree of radial symmetry around the fovea, and the extra band should be seen in many eyes, but was not demonstrated in published reports.[69,70] The band reported to be the rod OS tips has been seen only in retinal regions around the optic nerve and in only some eyes. A separation of the rod OS tips from the RPE in this area has not been described in histologic reports. An alternate explanation may be

advanced based on known histology.[23,58] Cones become wider and shorter with increasing distance from the fovea. However, there are curious patches of cones near the optic nerve that are much shorter and wider (8 μm) than elsewhere.[23,58] It is possible that these localized subpopulations of cones provide a different reflective level for Band 3 in this region leading to the ambiguity causing some to think the band was arising from the rods (Figure 8).

While the correspondence between the ellipsoid portion of the photoreceptors to Band 2 and the contact cylinder to Band 3 appears to be robust, the widths of the bands corresponding to the ELM and the RPE are somewhat less so. In the case of the ELM, the observed band width is broadened by the PSF of the OCT and is likely to originate from a thin structure. In addition, the log transform broadens any detected band. Thus, the LRP peak projected from the OCT to the drawing (Figure 6 and 7) is misleading and actually should be much narrower. The RPE width is harder to explain. In the perifoveal location, the width of the RPE band matches up fairly closely with the size of the RPE in the drawing. In the foveal location, the fourth band is much thicker than the RPE cell in the drawing. There are many possible explanations for this discrepancy, but one significant problem is that it is not known at present what, in addition to the RPE, is contained in the fourth band. There are regional differences in Bruch membrane and the choroid, and to the extent these are also contained in the fourth band, topographic thickness variations could occur.

This article represents a preliminary analysis comparing OCT-derived anatomical information with previously published data on outer retinal histology. The present study is a novel cross-check of established knowledge of retinal anatomy and compared that specific reflectance information obtained by OCT. Additional analysis of the imaging characteristics of OCT instruments and the reflective properties of boundaries was performed to provide supportive evidence. The results of this initial study suggest that names and anatomical structures commonly attributed to some of the hyperreflective bands visualized by OCT in the outer retina are not correct. The present study has the potential for numerous weaknesses. Interest in one structure or another in the outer retina varied over the years and no one paper or book described or measured all of the values needed for this article. Many studies were based on a limited number of eyes, and values reported may have been inaccurate. Another limitation is that our conclusions were drawn on the basis of images generated by and subject to the constraints of commercially available instruments. Other instruments may display the bands differently as OCT technology continues to evolve. This study was a hypothesis generation effort looking at broad principles and was not designed to evaluate specific OCT instruments or potential in subject variation related to age, gender, or race. Additional studies could include comparison between OCT in vivo with histologic correlative evaluations; these are currently underway. The impetus for these additional studies would not have occurred without first analyzing the possibility that the outer lines may have not been correct in the first place. Our goal is to develop nomenclature that is internally consistent and based on anatomical ground truth. Comprehensive and accurate measures of the width, spacing, and regional differences in OCT bands and candidate correlates for them in outer retina will be useful for reaching that goal. Given the clinical utility of OCT and the numerous assumptions concerning health and disease made based on OCT imaging, rapid and definitive resolution of these basic band assignments is important.

Acknowledgments

References

1. Huang D, Swanson EA, Lin CP, et al. Optical coherence tomography. Science. 1991; 254:1178–1181. [PubMed: 1957169]

2. Huang Y, Cideciyan AV, Papastergiou GI, et al. Relation of optical coherence tomography to microanatomy in normal and rd chickens. Invest Ophthalmol Vis Sci. 1998; 39:2405–2416. [PubMed: 9804149]

3. Huang Y, Cideciyan AV, Aleman TS, et al. Optical coherence tomography (OCT) abnormalities in rhodopsin mutant transgenic swine with retinal degeneration. Exp Eye Res. 2000; 70:247–251. [PubMed: 10655151]

4. Forte R, Cennamo GL, Finelli ML, de Crecchio G. Comparison of time domain Stratus OCT and spectral domain SLO/OCT for assessment of macular thickness and volume. Eye (Lond). 2009; 23:2071–2078. [PubMed: 19079147]

5. Kiernan DF, Hariprasad SM, Chin EK, et al. Prospective comparison of cirrus and stratus optical coherence tomography for quantifying retinal thickness. Am J Ophthalmol. 2009; 147:267–275. e2. [PubMed: 18929353]

6. Puliafito CA, Hee MR, Lin CP, et al. Imaging of macular diseases with optical coherence tomography. Ophthalmology. 1995; 102:217–229. [PubMed: 7862410]

7. Drexler W, Morgner U, Ghanta RK, et al. Ultrahigh-resolution ophthalmic optical coherence tomography. Nat Med. 2001; 7:502–507. [PubMed: 11283681]

8. Drexler W, Sattmann H, Hermann B, et al. Enhanced visualization of macular pathology with the use of ultrahigh-resolution optical coherence tomography. Arch Ophthalmol. 2003; 121:695–706. [PubMed: 12742848]

9. Ko TH, Fujimoto JG, Duker JS, et al. Comparison of ultrahigh- and standard-resolution optical coherence tomography for imaging macular hole pathology and repair. Ophthalmology. 2004; 111:2033–2043. [PubMed: 15522369]

10. [Accessed June 6, 2011] http://www.accessdata.fda.gov/cdrh_docs/pdf6/K063388.pdf

11. Srinivasan VJ, Ko TH, Wojtkowski M, et al. Noninvasive volumetric imaging and morphometry of the rodent retina with high-speed, ultrahigh-resolution optical coherence tomography. Invest Ophthalmol Vis Sci. 2006; 47:5522–5528. [PubMed: 17122144]

12. Srinivasan VJ, Monson BK, Wojtkowski M, et al. Characterization of outer retinal morphology with high-speed, ultrahigh-resolution optical coherence tomography. Invest Ophthalmol Vis Sci. 2008; 49:1571–1579. [PubMed: 18385077]

13. Zawadzki RJ, Jones SM, Olivier SS, et al. Adaptive-optics optical coherence tomography for high-resolution and high-speed 3D retinal in vivo imaging. Opt Express. 2005; 13:8532–8546. [PubMed: 19096728]

14. Puche N, Querques G, Benhamou N, et al. High-resolution spectral domain optical coherence tomography features in adult onset foveomacular vitelliform dystrophy. Br J Ophthalmol. 2010; 94:1190–1196. [PubMed: 20576764]

15. Gloesmann M, Hermann B, Schubert C, et al. Histologic correlation of pig retina radial stratification with ultrahigh-resolution optical coherence tomography. Invest Ophthalmol Vis Sci. 2003; 44:1696–1703. [PubMed: 12657611]

16. Krebs, W.; Krebs, I. Primate Retina and Choroid: Atlas of Fine Structure in Man and Monkey. New York, NY: Springer Verlag; 1991.

17. Hogan, MJ.; Alvarado, JA.; Weddell, JE. An Atlas and Textbook. Philadelphia, PA: W. B. Saunders; 1971. Histology of the Human Eye; p. 328-363.

18. Verhoeff FH. A hitherto undescribed membrane of the eye and its significance. R Lond Ophthalmic Hosp Rep. 1903; 15:309–319.

19. Wolff E. The external limiting membrane of the retina and its relation to Verhoeff's membrane. Trans Ophthalmol Soc U K. 1950; 60:61–67.

20. Joussen F, Spitznas M. The fine structure of the human retina at the ora serrata. Albrecht Von Graefes Arch Klin Exp Ophthalmol. 1972; 185:177–188. [PubMed: 4538828]

21. Feeney L. Intercellular junctions: sites of permeability barriers and cellular communication [editorial]. Invest Ophthalmol. 1974; 13:811–814. [PubMed: 4215036]

22. Borwein B, Borwein D, Medeiros J, McGowan JW. The ultrastructure of monkey foveal photoreceptors, with special reference to the structure, shape, size and spacing of the foveal cones. Am J Anat. 1980; 159:125–146. [PubMed: 7446444]

23. Curcio CA, Sloan KR, Kalina RE, Hendrickson AE. Human photoreceptor topography. J Comp Neurol. 1990; 292:497–523. [PubMed: 2324310]

24. Missotten L. Ultrastructure of ocular tissue. Bull Soc Belge Ophtalmol. 1964; 136:3–204. [PubMed: 14108488]

25. Anderson DH, Fisher SK, Steinberg RH. Mammalian cones: disc shedding, phagocytosis, and renewal. Invest Ophthalmol Vis Sci. 1978; 17:117–133. [PubMed: 415019]

26. Borwein B. Scanning electron microscopy of monkey foveal photoreceptors. Anat Rec. 1983; 205:363–373. [PubMed: 6837948]

27. Dowling JE. Foveal receptors of the monkey retina: fine structure. Science. 1965; 147:57–59. [PubMed: 14224526]

28. Steinberg RH, Wood I. Pigment epithelial cell ensheathment of cone outer segments in the retina of the domestic cat. Proc R Soc Lond B Biol Sci. 1974; 187:461–478. [PubMed: 4155505]

29. Rodieck, RW. The First Steps in Seeing. Sunderland, MA: Sinauer Associates; 1999.

30. Cohen AI. The fine structure of the extrafoveal receptors of the Rhesus monkey. Exp Eye Res. 1961; 1:128–136. [PubMed: 13880203]

31. Perkins GA, Ellisman MH, Fox DA. Three-dimensional analysis of mouse rod and cone mitochondrial cristae architecture: bioenergetic and functional implications. Mol Vis. 2003; 9:60–73. [PubMed: 12632036]

32. Rana MW, Taraszka SR. Monkey photoreceptor calycal processes and interphotoreceptor matrix as observed by scanning electron microscopy. Am J Anat. 1991; 192:472–477. [PubMed: 1781454]

33. Sidman RL. The structure and concentration of solids in photoreceptor cells studied by refractometry and interference microscopy. J Biophys Biochem Cytol. 1957; 3:15–30. [PubMed: 13416308]

34. Enoch, GM.; Tobey, FL. Vertebrate Photoreceptor Optics. New York, NY: Springer; 1981.

35. Polyak, SL. The Retina. Chicago, MA: University of Chicago; 1941.

36. Hoang Q, Linsenmeier RA, Chung C, Curcio CA. Photoreceptor inner segments in monkey and human retina: mitochondrial density, optics, and regional variation. Vis Neurosci. 2002; 19:395–407. [PubMed: 12511073]

37. Anderson DH, Fisher SK. The relationship of primate foveal cones to the pigment epithelium. J Ultrastruct Res. 1979; 67:23–32. [PubMed: 109622]

38. Hogan MJ, Wood I, Steinberg RH. Phagocytosis by pigment epithelium of human retinal cones. Nature. 1974; 252:305–307. [PubMed: 4431450]

39. Steinberg RH, Wood I, Hogan MJ. Pigment epithelial ensheathment and phagocytosis of extrafoveal cones in human retina. Philos Trans R Soc Lond B Biol Sci. 1977; 277:459–474. [PubMed: 16301]

40. Walls G. Human rods and cones: the state of knowledge. Arch Ophthalmol. 1934; 12:914–930.

41. Spitznas M, Hogan MJ. Outer segments of photoreceptors and the retinal pigment epithelium. Interrelationship in the human eye. Arch Ophthalmol. 1970; 84:810–819. [PubMed: 4321117]

42. Newman E, Reichenbach A. The Muller cell: a functional element of the retina. Trends Neurosci. 1996; 19:307–312. [PubMed: 8843598]

43. Bonilha VL, Rayborn ME, Bhattacharya SK, et al. The retinal pigment epithelium apical microvilli and retinal function. Adv Exp Med Biol. 2006; 572:519–524. [PubMed: 17249618]

44. Nishikawa S, Tamai M. Müller cells in the human foveal region. Curr Eye Res. 2001; 22:34–41. [PubMed: 11402377]

45. Distler C, Dreher Z. Glia cells of the monkey retina—II. Müller cells Vision Res. 1996; 36:2381–2394.

46. Bernstein MH. The interphotoreceptor matrix and the interphotoreceptor space of the vertebrate retina. Scan Electron Microsc. 1985:859–868. [PubMed: 2413523]

47. Sharma, RK.; Ehinger, B. Development and structure of the retina. In: Kaufman, PL.; Alm, A., editors. Adler's Physiology of the Eye. Clinical Application. 10. St. Louis, MO: Mosby; 2003. p. 319-347.

48. Tso MOM, Friedman E. The retinal pigment epithelium: I. Comparative histology. Arch Ophthalmol. 1967; 78:641–649. [PubMed: 4963693]

49. Krebs W, Krebs IP. Quantitative morphology of the primate peripheral retina (*Macaca irus*). Am J Anat. 1987; 179:198–208. [PubMed: 3303895]

50. Krebs W, Krebs IP. Quantitative morphology of the central fovea in the primate retina. Am J Anat. 1989; 184:225–236. [PubMed: 2750678]

51. Nguyen-Legros J, Hicks D. Renewal of photoreceptor outer segments and their phagocytosis by the retinal pigment epithelium. Int Rev Cytol. 2000; 196:245–313. [PubMed: 10730217]

52. Goldbaum MH, Madden K. A new perspective on Bruch's membrane and the retinal pigment epithelium. Br J Ophthalmol. 1982; 66:17–25. [PubMed: 7055538]

53. Williams CD, Rizzolo LJ. Remodeling of junctional complexes during the development of the outer blood-retinal barrier. Anat Rec. 1997; 249:380–388. [PubMed: 9372172]

54. Brill MH. Weber's law and perceptual categories: another teleological view. Bull Math Biol. 1983; 45:139–142. [PubMed: 6850156]

55. Drexler W. Ultrahigh-resolution optical coherence tomography. J Biomed Optics. 2004; 9:47–74.

56. Izatt, JA.; Choma, MA. Theory of optical coherence tomography. In: Drexler, W.; Fujimoto, J., editors. Optical Coherence Tomography: Technology and Applications. New York, NY: Springer; 2008. p. 47-72.

57. Ward RK. Restoration of differently blurred versions of an image with measurement errors in the PSF's. IEEE Trans Image Process. 1993; 2:369–381. [PubMed: 18296224]

58. Curcio CA, Saunders PL, Younger PW, Malek G. Peripapillary chorioretinal atrophy: Bruch's membrane changes and photo-receptor loss. Ophthalmology. 2000; 107:334–343. [PubMed: 10690836]

59. Toth CA, Narayan DG, Boppart SA, et al. A comparison of retinal morphology viewed by optical coherence tomography and by light microscopy. Arch Ophthalmol. 1997; 115:1425–1428. [PubMed: 9366674]

60. Chauhan DS, Marshall J. The interpretation of optical coherence tomography images of the retina. Invest Ophthalmol Vis Sci. 1999; 40:2332–2342. [PubMed: 10476800]

61. Giovannini A, Amato G, Mariotti C, Scassellati-Sforzolini B. Optical coherence tomography in the assessment of retinal pigment epithelial tear. Retina. 2000; 20:37–40. [PubMed: 10696745]

62. Sarraf D, Reddy S, Chiang A, et al. A new grading system for retinal pigment epithelial tears. Retina. 2010; 30:1039–1045. [PubMed: 20458264]

63. Lujan BJ, Rosenfeld PJ, Gregori G, et al. Spectral domain optical coherence tomographic imaging of geographic atrophy. Ophthalmic Surg Lasers Imaging. 2009; 40:96–101. [PubMed: 19320296]

64. Shields CL, Materin MA, Walker C, et al. Photoreceptor loss overlying congenital hypertrophy of the retinal pigment epithelium by optical coherence tomography. Ophthalmology. 2006; 113:661–665. [PubMed: 16581426]

65. Ahlers C, Gotzinger E, Pircher M, et al. Imaging of the retinal pigment epithelium in age-related macular degeneration using polarization-sensitive optical coherence tomography. Invest Ophthalmol Vis Sci. 2010; 51:2149–2157. [PubMed: 19797228]

66. Cense B, Gao W, Brown JM, et al. Retinal imaging with polarization-sensitive optical coherence tomography and adaptive optics. Opt Express. 2009; 17:21634–21651. [PubMed: 19997405]

67. Götzinger E, Pircher M, Geitzenauer W, et al. Retinal pigment epithelium segmentation by polarization sensitive optical coherence tomography. Opt Express. 2008; 16:16410–16422. [PubMed: 18852747]

68. Zawadzki RJ, Choi SS, Jones SM, et al. Adaptive optics-optical coherence tomography: optimizing visualization of microscopic retinal structures in three dimensions. J Opt Soc Am A Opt Image Sci Vis. 2007; 24:1373–1383. [PubMed: 17429483]

69. Srinivasan VJ, Adler DC, Chen Y, et al. Ultrahigh-speed optical coherence tomography for three-dimensional and en face imaging of the retina and optic nerve head. Invest Ophthalmol Vis Sci. 2008; 49:5103–5110. [PubMed: 18658089]

70. Srinivasan VJ, Chen Y, Duker JS, Fujimoto JG. In vivo functional imaging of intrinsic scattering changes in the human retina with high-speed ultrahigh resolution OCT. Opt Express. 2009; 17:3861–3877. [PubMed: 19259228]
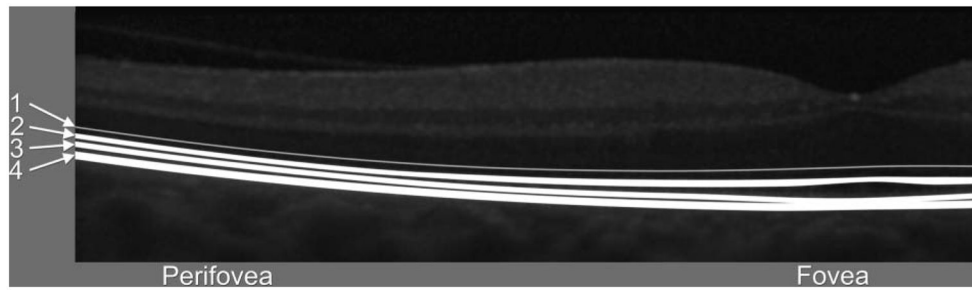
Fig. 1.
Drawing of the outer hyperreflective bands overlaid on a representative spectral-domain OCT scan of a normal macula. Each of the bands has had different anatomical correlations proposed over time, with varying designations by research group and time period. Typical attributions are as follows: Band 1, the ELM; Band 2, the boundary between the ISs and OSs of the photoreceptors; Band 3, the OS tips or Verhoeff membrane; Band 4, the RPE, possibly including Bruch membrane and the choriocapillaris.
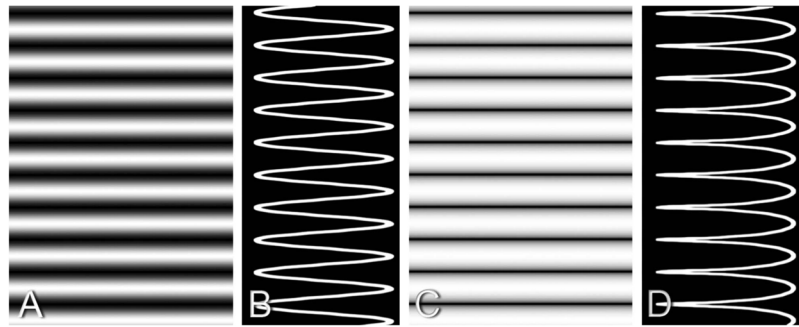
Fig. 2.
Alterations in band appearance caused by logarithmic transformation. **A**. A gray scale sine wave shows equivalent width bands of light and dark, with a gradual transition between. A log transform of (**A**) results in (**C**). This type of transformation is commonly done to display information from OCT scans. **B**. The longitudinal intensity profile through the image shown in (**A**) reveals the expected sine wave pattern. **D**. The longitudinal density profile taken through (**C**) reveals a distortion of gray scale values and broadening of the bright bands induced by the log transform.
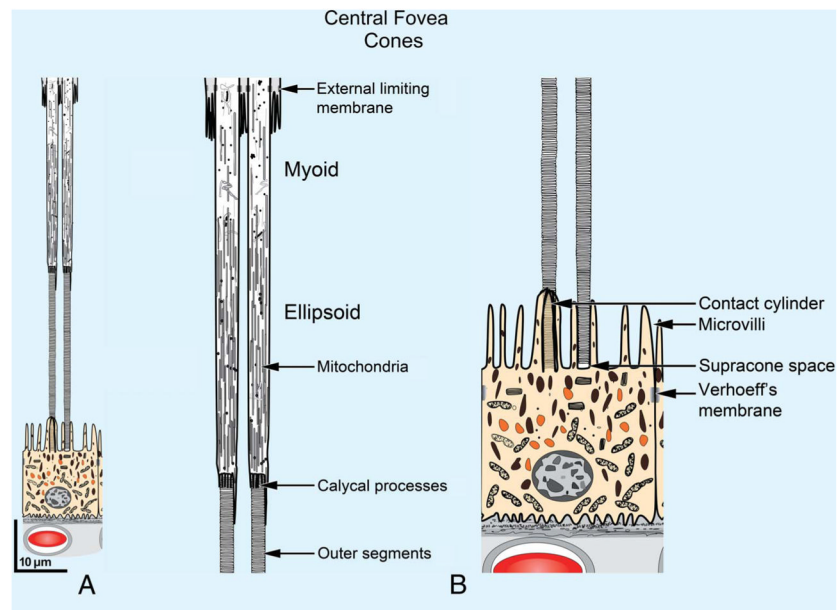
Fig. 3.
A. Lower magnification and (**B**) high magnification in two parts. A scale drawing of the outer retina showing cones in the central fovea (**A**, low magnification). In (**B**) (higher magnification) the Muller cells form junctional complexes with the photoreceptors that when viewed in aggregate are called the ELM. In reality, it is not a membrane, limiting or otherwise. The foveal cones are narrow and cylindrical, like rods. The inner portion of the IS is called the myoid and the outermost division is the ellipsoid, which contain numerous thin mitochondria. Extending over the proximal OS are fine cytoplasmic extensions called the calycal processes. The RPE has small apical extensions called microvilli. The OS continue to the RPE and are enveloped in specialized apical processes forming a contact cylinder (left cone). A small gap (the supracone space) is present between the outermost part of the OS and the RPE, seen in the cross-sectional view (right). Retinal pigment epithelial cells have junctional complexes (drawn larger than scale for clarity) formed with neighboring RPE cells. The confluence of these complexes as seen by light microscopy is called, in a manner analogous to the ELM, Verhoeff membrane.
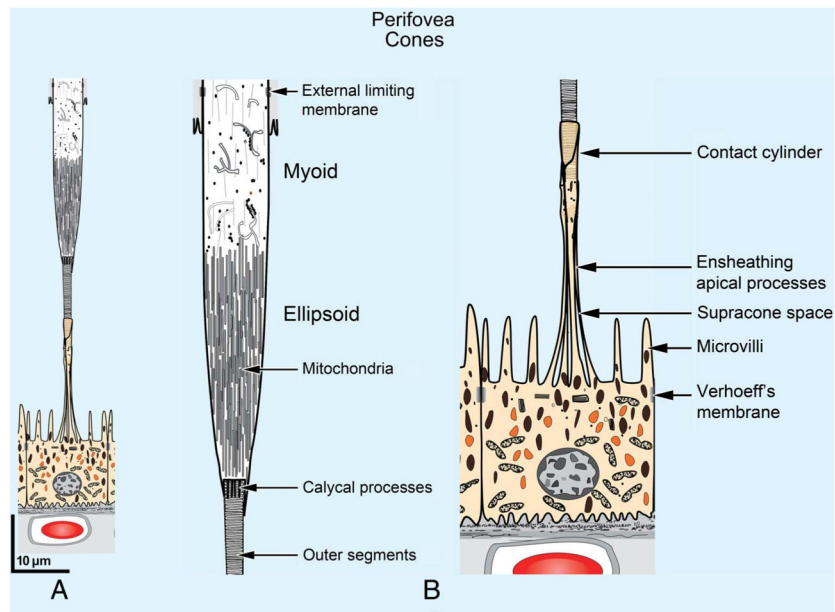
Fig. 4.

A. Lower magnification and (**B**) high magnification in two parts. IS, perifoveal cone. Cone IS widen with greater eccentricity from the foveal center. Mitochondria fill approximately 75% of the ellipsoid volume and account for the enormous oxygen use by photoreceptors. Like foveal cones, perifoveal cones have small cytoplasmic extensions called the calycal processes that extend over the innermost OSs. The ELM designates junctional complexes named for their appearance by light microscopy. Outer segments of cones outside of the central macula stop well short of the underlying RPE cells. Specialized apical extensions arise from the RPE to encase the outer one third of OS length, recognized here by the faint obscuration of the OS disks. These ensheathing apical processes have cellular machinery not ordinarily found in microvilli such as ribosomes and mitochondria. Shed OS are moved back to the RPE cell body for phagocytosis through the supracone space. The RPE apical junctional processes are labeled according to their appearance on light microscopy, Verhoeff membrane.
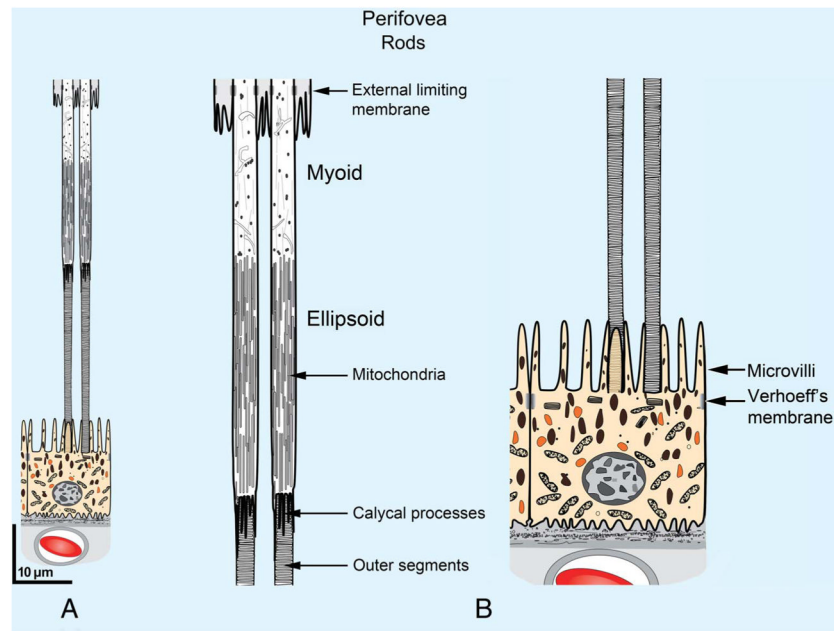
Fig. 5.
A. Lower magnification and (**B**) higher magnification in two parts. Rods are present outside of the central fovea. The rod IS is composed of the myoid and ellipsoid sections. Both rod IS width and mitochondrial packing density are much less than cones in the perifovea. The cytoplasmic extensions of the calycal process are longer for rods than cones. The OS tips are surrounded by fine apical extensions, analogous to the contact cylinder of cones (rod at left). Rods extend down to contact the RPE cells in a cross-sectional view (rod at right).
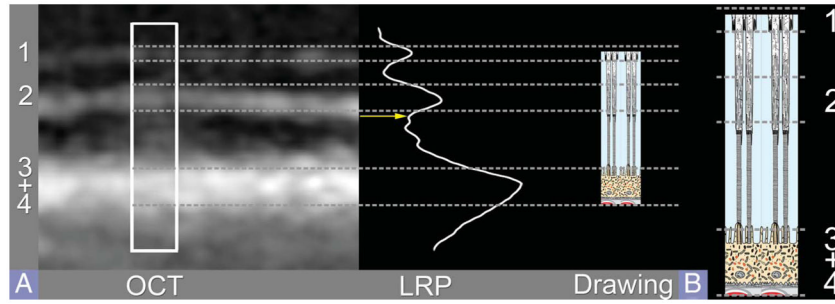
Fig. 6.
A. A representative OCT image of the fovea showing the outer bands. In the central fovea, the third band appears to blend in with the fourth band. The highlighted box is a 10-pixel-wide region used to create the LRP. The dashed lines show the agreement between the hyperreflective bands and the LRP. These dashed lines extend to a drawing scaled to coincide with the peak of the band attributed to the ELM (Band 1) and the junctional complexes between the Muller cells and the photoreceptors in the drawing. The dashed lines represent the full-width at half maximum point of the LRP curve for the ELM. The second band is centered over and encompasses the ellipsoid section of the photoreceptors. Note that the local nadir of the LRP colocalizes near the IS/OS boundary (arrow). The outer hyperreflective band, formed by the overlap of the third and fourth bands corresponds to the region extending from the contact cylinders to slightly sclerad to Bruch membrane. **B**. These relationships are shown in a magnified version in the inset at right.
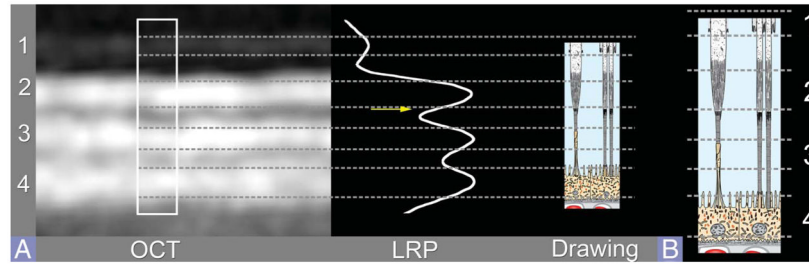
Fig. 7.
A. A representative OCT of the perifoveal region 2 mm temporal to the center of the fovea showing the outer bands. The highlighted box is a region 10 pixels wide that was used to create the LRP. The dashed lines from the OCT through the LRP were continued to the drawing. The first band of the OCT represents the ELM and was aligned with the junctional complexes between the Muller cells and the photoreceptors. The dashed lines represent the full-width at half maximum point of the LRP curve for the ELM. The second band corresponded very closely with the ellipsoid section of the IS. The third band encompassed the region of the cone OS/contact cylinder region. The fourth band was aligned to the RPE with the peak of the LRP corresponding to the inner one third of the RPE cells, which is where the melanosomes are more commonly found. As opposed to the comparison involving the fovea, the outer portion of the fourth band does not extend past Bruch membrane in this region. Note the boundary between the IS and OS is near the lowest local reflectivity in the LRP (arrow). **B**. These relationships are shown in a magnified version in the inset at right.
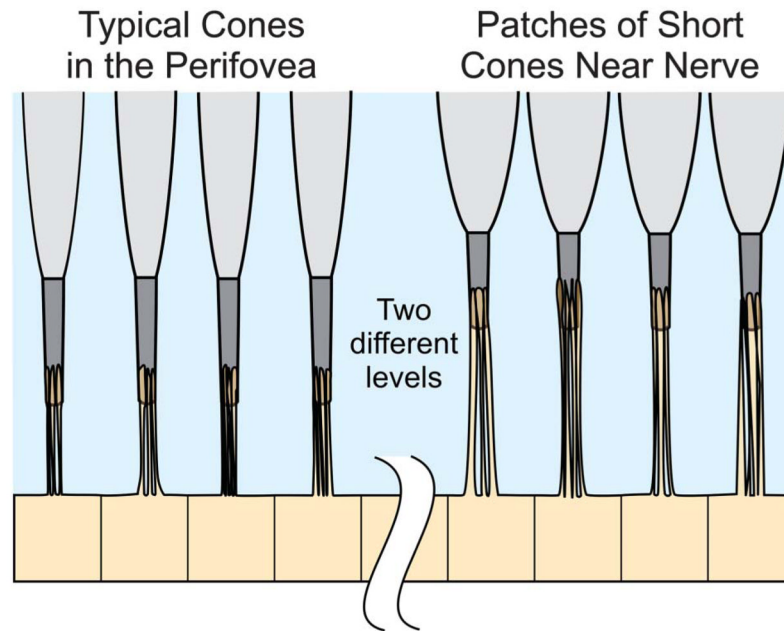
Fig. 8.
Near the nerve, there are isolated patches of short, wide cones seen in otherwise normal donor eyes.[26] Because of the displacement of the contact cylinder anteriorly, it is possible for more than one level to be observed. The rods are not shown in this drawing.

Table 1

Outer Retinal Anatomy

Cell	Feature	Parameter[*]	Value	References
Cones	ELM[†]	Appearance		16,17,22
	Mitochondria	Number	200–300	16,17,23–29
	Mitochondria	Diameter, μm	0.15–0.30	24,30,31
	Mitochondria	Length, μm	3	24,30
	Calycal processes	Appearance		24
	Calycal processes	Length, μm	1	22,26
	Calycal processes	Number[‡]	11.6	32
	Ciliary backbone	Appearance		22
	IS myoid	Refractive index	1.3605	33
	IS ellipsoid	Refractive index	1.394	33,34
	OS	Refractive index	1.39	33,34
Cones, foveal	IS myoid	Diameter, μm	2	16,17,23,29,35,36
	IS myoid	Length, μm	14	16,17,23,29,35,36
	IS ellipsoid	Length, μm	20	16,17,23,29,35,36
	OS	Length, μm	35	16,17,23,29,32,35,36
	Supracone space[§]	Distance, μm	1	16,17,29,37
Cones, perifoveal[¶]	IS myoid	Diameter, μm	5	16,17,23,29,35,36
	IS myoid	Length, μm	13	16,17,23,29,35,36
	IS ellipsoid	Length, μm	16	16,17,23,29,35,36
	Supracone space[§]	Distance, μm	16	25
	Contact cylinder[**]	Length, μm	4	16,17,38
	Shed OS disks within ensheathing processes	Appearance		25,38–40
Rods[††]	ELM[†]	Appearance		26
	Mitochondria	Number	40	16,17,24,30,31
	Mitochondria	Diameter, μm	0.15–0.3	24,30,36
	Mitochondria	Length, μm	3	24
	Calycal processes	Appearance		22,26
	Calycal processes	Length, μm	0.7–3	32
	Calycal processes	Number[‡]	2.9	32
	IS myoid	Diameter, μm	2	16,17,29,36
	IS myoid	Length, μm	12	16,17,29,36
	IS ellipsoid	Length, μm	17	16,17,29,36
	Connecting cilia	Diameter, μm	0.25	16,22,24
	Connecting cilia	Length, μm	1	16,22,24
	Ciliary backbone	Appearance		26
	OS	Length, μm	32	16,17,29,36

Cell	Feature	Parameter[*]	Value	References
	OS tip–RPE separation	Distance, μm	<1	25,41
	IS myoid	Refractive index	1.3606	33
	IS ellipsoid	Refractive index	1.398	33
	OS	Refractive index	1.408	33
Muller cells[‡‡]	ELM[†]	Appearance		16,17,26
	Microvilli	Appearance		16,17,26,28,46
RPE[§§]	Cell body	Diameter, μm	14	35,47
	Nucleus	Diameter, μm	5	48
	Height[¶¶]	Appearance		35
	Ensheathment [***]	Appearance		25,39,40
	Organelles [†††]	Appearance		25,39
	Microvilli	Length, μm	5–7	35,47
	Contact with rods and cones	Appearance		49,50
	OS phagocytosis	Appearance		51
	Verhoeff membrane[‡‡‡]	Appearance		18,19,52,53

[*] Length refers to vertical height (in the direction of light rays). Diameter refers to horizontal cross-sectional diameter (parallel to the image plane). Distance describes a compartment.

[†] Zonulae adherens.

[‡] Per cross-sectional profile.

[§] Compartment between tip of OS and RPE.

[¶] Two millimeters from the foveal center.

[**] Overlap between cone OS and ensheathing processes of RPE.

[††] For general information about rods, see Krebs and Krebs,[16] Hogan et al,[17] Missotten,[24] Anderson et al,[25] and Rodieck.[29]

[‡‡] For general information about Muller cells, see Krebs and Krebs,[16] Hogan et al,[17] Rodieck,[29] Newman and Reichenbach,[42] Bonilha et al,[43] Nishikawa and Tamai,[44] Distler and Dreher.[45]

[§§] For general information about RPE, see Krebs and Krebs,[16] Hogan et al,[17] and Borwein et al.[22]

[¶¶] Height is greater in fovea than periphery.

[***] Extrafoveal cones are ensheathed by the contact cylinder (see compartment between tip of OS and RPE).

[†††] In elongated apical processes.

[‡‡‡] A belt of junctional complexes that separate apical and basolateral RPE membrane domains and form part of the blood–retina barrier.